Method of linear combination of structural motifs for surface and step energy calculations: Application to GaAs(001)

S. B. Zhang and Alex Zunger
National Renewable Energy Laboratory, Golden, Colorado 80401
(Received 2 February 1995)

First-principles calculations of the atomic structure and formation energies of semiconductor surfaces and surface steps are often complicated by the existence of complex structural patterns. We suggest here a simpler, algebraic (not differential) approach that is based on two observations distilled from previous first-principles calculations. *First*, a relatively large collection of equilibrium structures of surfaces and bulk point defects can be built from a limited number of recurring local ''structural motifs,'' including for GaAs tetrahedrally bonded Ga and As and miscoordinated atoms such as threefold-coordinated pyramidal As. *Second*, the structure is such that band-gap levels are emptied, resulting in charged miscoordinated atoms. These charges compensate each other. We thus express the total energy of a given surface as a sum of the energies of the motifs, and an electrostatic term representing the Madelung energy of point charges. The motif energies are derived by fitting them to a set of pseudopotential total-energy calculations for *flat* GaAs(001) surfaces and for point defects in *bulk* GaAs. This set of parameters is shown to suffice to reproduce the energies of *other* (001) surfaces, calculated using the same pseudopotential approach. Application of the ''linear combination of structural motif'' (LCSM) method to flat GaAs(001) surfaces reveals the following: (i) The observed $h(2\times3)$ surface may be a disordered $c(8\times6)$ surface. (ii) The observed (2×6) surface is a metastable surface, only 0.03 eV/(1×1) higher than the $\alpha(2\times4)$ surface having the same surface coverage. (iii) We confirm the recent suggestion by Hashizume *et al.* that the observed $\gamma(2\times4)$ phase of the (2×4) surface is a mixture of the $\beta2(2\times4)$ and $c(4\times4)$ surfaces. In particular, we examined an 8×7 surface structure which has a lower energy than the earlier proposed $\gamma(2\times4)$ structure. Application of the LCSM method to prototype *steps* on the GaAs(001)-(2×4) surface is illustrated, comparing the LCSM results directly to pseudopotential results.

I. INTRODUCTION: THE BASIC IDEA

With the advent of scanning tunneling microscopy (STM) and spectroscopy techniques, it is now possible to examine in detail the adequacy of the theoretically proposed atomic-scale structures of surfaces. While it is possible to directly calculate from first principles the total energies of various flat surface structures, and in some simple cases even the relative energies of the structurally more complex surface steps,[1] these first-principles calculations suggest a simpler, approximate approach to such time-consuming calculations. Two central observations are pertinent here: *First*, in a relatively large collection of proposed structures of III-V (001) surfaces[2–4] (Figs. 1–3), as well as in calculated structures of bulk point defects,[2–5] the cation and anion atoms assume only a small number of local structures, to be named here ''structural motifs.'' For example, all the local-density approximation (LDA) derived GaAs(001) surface structures in Figs. 1–3 can be thought of as being built from different combinations of the seven structural motifs in Fig. 4: Denoting the local coordination number by superscripts, these motifs include tetrahedrally bonded $Ga^{(4)}$ and $As^{(4)}$, pyramidal $As^{(3)}$, planar $Ga^{(3)}$, and bridge site $Ga^{(2)}$. In addition to the ''one-site motifs,'' ''two-site motifs'' are also needed here to account for ''wrong bonds'' (i.e., the Ga-Ga and As-As bonds). *Second*, previous studies on GaAs(001) surfaces[6] reveal equilibrium atomic structures for which all electronic shells (or gap levels) are either completely full or completely empty. (We refer to this as the generalized ''octet rule.'') Application of this rule to candidate surface structures predicts a set of point charges on the various surface atoms. While assignment of these charges leads to an insulating surface, in satisfaction of the octet rule, this rule does not automatically guarantee overall charge neutrality. Deviations from neutrality would have led to a divergent electrostatic energy (''Coulomb catastrophe'') for two-dimensional systems (i.e., surfaces), as well as for one-dimensional systems (i.e., steps). However, by combining oppositely charged atoms, e.g., the $+\frac{3}{4}$ electron $Ga^{(3)}$ donor with the $-\frac{3}{4}$ electron $As^{(3)}$ acceptor, we can restore charge neutrality through ''charge compensation.'' Concurrently, we gain the energy resulting from charge transfer from the near-conduction-band minimum $Ga^{(3)}$ donor level to the near-valence-band maximum $As^{(3)}$ acceptor level,[7] as well as the Madelung energy resulting from the interaction of the $+\frac{3}{4}$ and $-\frac{3}{4}$ point charges. Stable (or nearly stable) surface structures produced by LDA total-energy calculations on GaAs(001) surfaces appear to always obey the above noted ''charge-compensation octet rule.''[3,4] This appears to result in the rather small number of ''local structural motifs'' (Fig. 4) at the, e.g., (001), surfaces. These observations suggest then a simple strategy for identifying the atomic topology of stable surface or steps and estimating their formation energies. (The method does not provide the precise relaxed atomic positions, i.e., ''geometry,'' but does give the basic structural elements, i.e., ''topology.'') In this paper, we describe the basic method (Sec. II) and then apply this ''linear combination of structural motifs'' (LCSM) method to (i) 12 reconstructions on the *flat* GaAs(001) surface, where comparison to LDA formation en-

 © 1996 The American Physical Society

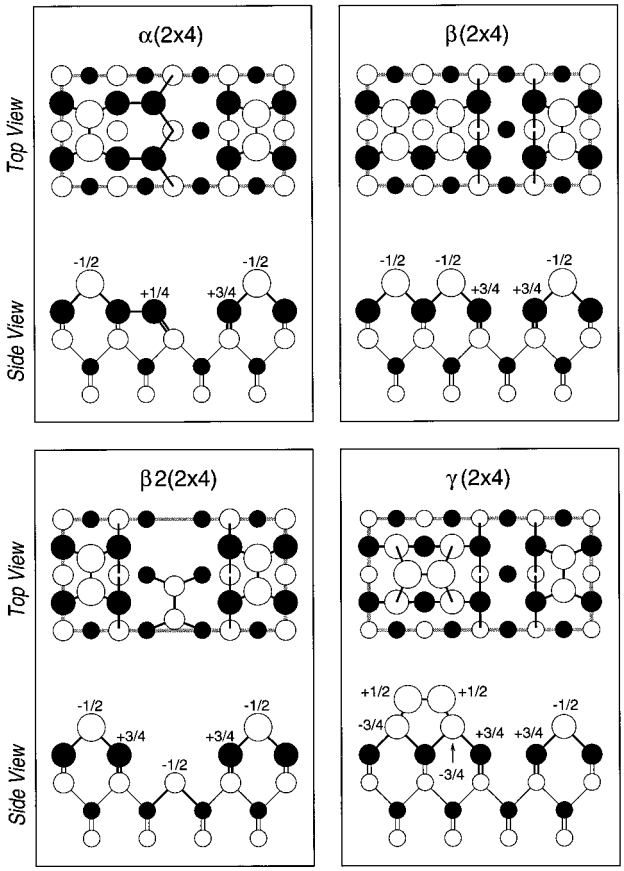

FIG. 1. Top and side views of four ''flat'' GaAs surface structures depicted in a ball-stick model. The filled and open circles are Ga and As, respectively, with descending sizes from the top surface layer. In the top view, the thick shaded lines denote surface unit cells. In the side view, the thin bonds indicate the bulk bonds that are not shown in the top views and the double lines indicate that the atom has two bonds in the direction perpendicular to the paper. The numbers denote the point charge assigned according to the octet rule (Table I).

ergies are presented (Sec. III); (ii) additional reconstruction models for GaAs(001) that are too computer intensive for current pseudopotential LDA calculations (Sec. IV); (iii) prototypical steps on GaAs(001)-$\beta 2(2\times4)$ surface (Sec. V). We find that the LCSM method provides good quantitative estimates of the formation energies and, at the same time, distills essential features from complex LDA calculations.

II. THE METHOD OF LINEAR COMBINATION OF STRUCTURAL MOTIFS

Based on the discussion in the Introduction, we postulate that the total energy of a system $\boldsymbol{\sigma}$ (=bulk point defects, surfaces, or steps) can be written as

$$E(\boldsymbol{\sigma},\boldsymbol{\mu}_{\mathscr{R}})=E_{\mathrm{LCSM}}(\boldsymbol{\sigma})+E_{\mathrm{Mad}}(\boldsymbol{\sigma})+E_{\mathscr{R}}(\boldsymbol{\sigma},\boldsymbol{\mu}_{\mathscr{R}}), \quad (1)$$

where

$$E_{\mathrm{LCSM}}(\boldsymbol{\sigma})=\sum_{M}\ \omega_M(\boldsymbol{\sigma})\epsilon_M \quad (2)$$

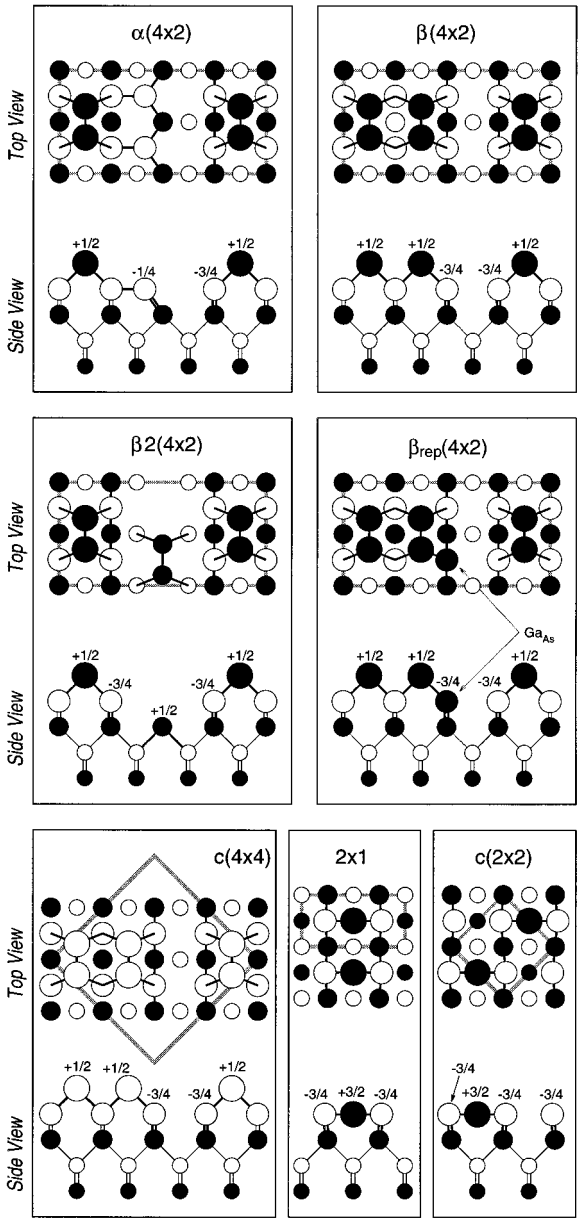

FIG. 2. Top and side views of seven additional ''flat'' GaAs surface structures. The legends are the same as in Fig. 1.

is a linear combination of structural motif energies ϵ_M with $\omega_M(\boldsymbol{\sigma})$ being the frequency of occurrence of motif M. We use the same characteristic motif energy ϵ_M for motif M, irrespective of the identity of its neighbors. The effects of different nearest-neighbor atoms are implemented through two-site ''wrong bond'' motifs and by the long-range interactions described electrostatically by a Madelung energy,

$$E_{\mathrm{Mad}}(\boldsymbol{\sigma})=\frac{1}{2\epsilon}\sum_{i,j}{}'\ Q_iQ_j/|R_i-R_j|. \quad (3)$$

Here, Q_i is the charge of the ith atom at position R_i and ϵ is the effective dielectric constant (=13 for bulk GaAs and to be determined for surfaces). Table I lists the various local motifs M, indicating in some cases in square brackets their nearest-neighbor atoms. Note that the identity of atoms in the

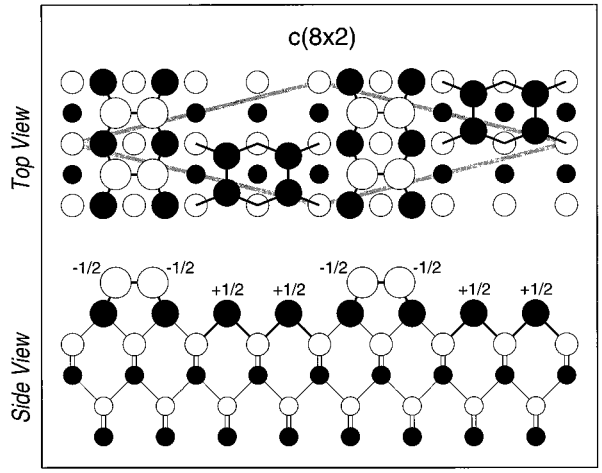

FIG. 3. Top and side views of the "flat" GaAs $c(8\times2)$ surface structure. The legends are the same as in Fig. 1.

nearest-neighbor shell to a given central site can vary, e.g., threefold $Ga^{(3)}$ can have either 3As, or $Ga^{(4)}$+2As, or $As^{(4)}$+2Ga neighbors. While the one-site motif energy $\epsilon_M[Ga^{(3)}]$ is constant in all of these cases, the charge $Q[Ga^{(3)}]$ does depend on the identity of the nearest neighbors, through application of the octet rule. Appendix A (Ref. 8) illustrates how the application of the octet rule leads to given point charges Q_i used in Eq. (3). Table I summarizes the values of Q_i for all the motifs used in the present work, including various choices of their neighbors. The bottom halves of Figs. 1–3 show these point charges for each type of surface atoms on the various surface structures. It is important to notice that in Eq. (2), the energy ϵ_M of a motif corresponds to an average $\epsilon_M \sim \Sigma_\sigma E(\sigma)\omega_M^{-1}(\sigma)$ over all energies $E(\sigma)$ in which motif M is embedded. Thus, we cannot interpret a motif as a geometrical entity with given bond lengths and angles, but rather as a topological entity defined through Eq. (2). Furthermore, we cannot speak of motifs changing their shape or charge when their (distant) neighbors change, since ϵ_M is already an average.

The last term in Eq. (1) is the "reservoir energy,"

$$E_{\mathscr{R}}(\boldsymbol{\sigma},\mu_{\mathscr{R}}) = \sum \mu_{\mathscr{R}} N_{\mathscr{R}}. \tag{4}$$

We assume that the system $\boldsymbol{\sigma}$ is in equilibrium with a reservoir $\mathscr{R}$, containing N_{Ga} of Ga atoms and N_{As} of As atoms with chemical potentials μ_{Ga} and μ_{As}, and N_e of electrons with a Fermi energy μ_e. The term of Eq. (4) is needed in order to account for both material and electron balance in a chemical reaction $\boldsymbol{\sigma}_0 \rightarrow \boldsymbol{\sigma}$.[9] In this case, the system formation energy can be written as

$$\begin{aligned}\Delta E(\boldsymbol{\sigma},\mu_{\mathscr{R}}) &= E(\boldsymbol{\sigma},\mu_{\mathscr{R}}) - E(\boldsymbol{\sigma}_0,\mu_{\mathscr{R}}) \\ &= \Delta E_{\mathrm{LCSM}}(\boldsymbol{\sigma}) + \Delta E_{\mathrm{Mad}}(\boldsymbol{\sigma}) + \Delta E_{\mathscr{R}}(\boldsymbol{\sigma},\mu_{\mathscr{R}}),\end{aligned} \tag{5}$$

where Δ denotes the appropriate *difference*. For example, formation of a Ga vacancy in bulk GaAs leads to the capture of three electrons from the electron reservoir (the "Fermi sea") and to the ejection of a Ga atom into the Ga reservoir. The formal reaction is

$$3e^- + \mathrm{Ga}^0_{\mathrm{Ga}} \rightarrow V^{3-}_{\mathrm{Ga}} + \mathrm{Ga}\ \ (\text{at reservoir}). \tag{6}$$

Denoting the formation energy of an *isolated* Ga vacancy by $\Delta E(V^{3-}_{\mathrm{Ga}}) = \Delta E_{\mathrm{LCSM}}(V^{3-}_{\mathrm{Ga}}) + \Delta E_{\mathrm{Mad}}(V^{3-}_{\mathrm{Ga}})$, the formation energy corresponding to the vacancy in *equilibrium* with the reservoirs [Eq. (6)] is thus

$$\Delta E = \Delta E(V^{3-}_{\mathrm{Ga}}) + \mu_{\mathrm{Ga}} - 3\mu_e, \tag{7}$$

TABLE I. Charge assignments in units of the absolute value of the electron charge (e) for various atoms. The square brackets in the second column denote the nearest neighbors to a given atom. Lines 1–6 apply to "normal site" atoms (i.e., Ga on a Ga site and As on an As site) without surface rebonding, while lines 7–10 apply to normal site atoms, with surface rebonding, and lines 11–14 apply to "antisite" atoms (i.e., Ga on an As site and As on a Ga site) regardless of surface rebonding.

Case number	Atom	Q (e)	Remark
1.	$Ga^{(4)}$	0	
2.	$As^{(4)}$	0	
3.	$Ga^{(3)}$ [3As]	$+\frac{3}{4}$	As=$As^{(2)}$, $As^{(3)}$, or $As^{(4)}$
4.	$As^{(3)}$ [3Ga]	$-\frac{3}{4}$	Ga=$Ga^{(2)}$, $Ga^{(3)}$, or $Ga^{(4)}$
5.	$Ga^{(2)}$	$+\frac{3}{2}$	
6.	$As^{(2)}$	$+\frac{5}{2}$	does not exit
7.	$Ga^{(3)}$ [$Ga^{(4)}$+2As]	$+\frac{1}{4}$	As=$As^{(3)}$ or $As^{(4)}$
8.	$As^{(3)}$ [$As^{(4)}$+2Ga]	$-\frac{1}{4}$	Ga=$Ga^{(3)}$ or $Ga^{(4)}$
9.	$Ga^{(3)}$ [$Ga^{(3)}$+2As]	$+\frac{1}{2}$	As=$As^{(3)}$ or $As^{(4)}$
10.	$As^{(3)}$ [$As^{(3)}$+2Ga]	$-\frac{1}{2}$	Ga=$Ga^{(3)}$ or $Ga^{(4)}$
11.	$Ga^{(4)}_{\mathrm{As}}$	-2	
12.	$As^{(4)}_{\mathrm{Ga}}$	$+2$	
13.	$Ga^{(3)}_{\mathrm{As}}$		$Q[Ga^{(3)}_{\mathrm{As}}]=Q[As^{(3)}_{\mathrm{As}}]$
14.	$As^{(3)}_{\mathrm{Ga}}$		$Q[As^{(3)}_{\mathrm{Ga}}]=Q[Ga^{(3)}_{\mathrm{Ga}}]$

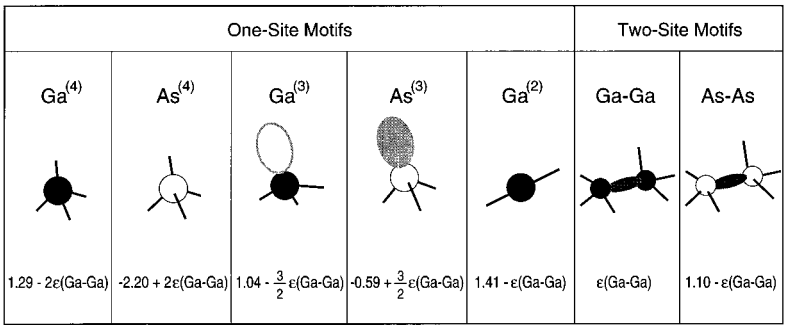

FIG. 4. Local structural motifs are shown schematically along with the motif energies, ϵ_M (in eV) relative to the energy of the Ga-Ga bond, ϵ(Ga-Ga). The reference corresponds to all the Ga and As atoms in their solid forms [i.e., μ (solid Ga)$=\mu$ (solid As)$=0$]. We use filled circles to denote Ga atoms and open circles to denote As atoms. The empty dangling bond orbital of $Ga^{(3)}$ and the filled dangling-bond orbital of $As^{(3)}$, as well as the Ga-Ga and As-As "wrong bonds," are also indicated.

so in Eq. (5) $\Delta N_{\rm Ga}=1$ and $\Delta N_e=-3$. We assume that the system $\boldsymbol{\sigma}$ is also in equilibrium with *bulk* GaAs,[10] leading to the constraint

$$\mu_{\rm Ga}+\mu_{\rm As}=\mu_{\rm GaAs}=-\Delta H, \tag{8}$$

where $\Delta H=[E(\text{Ga solid})+E(\text{As solid})]-E(\text{bulk GaAs})=0.92$ eV is the heat of formation of bulk GaAs calculated using LDA.[3] Equation (8) then allows us to eliminate a single variable, i.e., $\mu_{\rm As}$, and to express the reservoir energy as $\Delta E_{\mathscr{R}}(\boldsymbol{\sigma},\mu_{\rm Ga},\mu_e)$. This gives

$$\Delta E_{\mathscr{R}}(\boldsymbol{\sigma},\mu_{\rm Ga},\mu_e)=[\Delta N_{\rm Ga}(\boldsymbol{\sigma})-\Delta N_{\rm As}(\boldsymbol{\sigma})]\mu_{\rm Ga} -\Delta N_{\rm As}(\boldsymbol{\sigma})\Delta H+\Delta N_e(\boldsymbol{\sigma})\mu_e. \tag{9}$$

The deposition of solid Ga [if $\mu_{\rm Ga}$ exceeds $\mu_{\rm Ga}$(solid Ga)] and deposition of solid As [if $\mu_{\rm As}$ exceeds $\mu_{\rm As}$ (solid As)] provide sufficient conditions limiting the range of the atomic chemical potentials $\mu_{\rm Ga}$ and $\mu_{\rm As}$. These conditions, along with Eq. (8), set the range for the Ga chemical potential: $-\Delta H\leqslant\mu_{\rm Ga}\leqslant 0$. The range of the Fermi energy is bound by the band gap of GaAs, i.e., $0\leqslant\mu_e\leqslant E_g=1.5$ eV (see Ref. 5). The final form of the formation energy is then

$$\Delta E(\boldsymbol{\sigma},\mu_{\rm Ga},\mu_e)=\sum_M \Delta\omega_M(\boldsymbol{\sigma})\epsilon_M+\Delta E_{\rm Mad}(\boldsymbol{\sigma}) +\{[\Delta N_{\rm Ga}(\boldsymbol{\sigma})-\Delta N_{\rm As}(\boldsymbol{\sigma})]\mu_{\rm Ga} -\Delta N_{\rm As}(\boldsymbol{\sigma})\Delta H+\Delta N_e(\boldsymbol{\sigma})\mu_e\}. \tag{10}$$

Except for the case of bulk point defects, the charge-compensation octet rule $\Sigma_i Q_i=0$ applies. The latter equation implies $\Delta N_e(\boldsymbol{\sigma})=0-0$ in Eq. (10). Thus, the surface and step formation energies are independent of μ_e, so $\Delta E=\Delta E(\boldsymbol{\sigma},\mu_{\rm Ga})$.

Considering Eq. (10), for each candidate system $\boldsymbol{\sigma}$ with respect to the reference system $\boldsymbol{\sigma}_0$, we know $\{\Delta\omega_M\}$ (by counting motifs), as well as $(\Delta N_{\rm Ga}-\Delta N_{\rm As})$, $\Delta N_{\rm As}$, and ΔN_e (by counting atoms and electrons) and the charge $\{Q_i\}$ (see Appendix A and Table I). The unknowns are the surface dielectric constant ϵ_s and the motif energies $\{\epsilon_M\}$. We will extract ϵ_s and $\{\epsilon_M\}$ by fitting Eq. (10) to a set of LDA calculations on octet bulk point defects (i.e., those bulk point defects whose gap levels are empty) and on nominally flat surfaces. The reliability of the LCSM approach will then be tested by its ability to reproduce LDA energies of surface structures *not* used in the fit. Once the convergence of Eq. (10) is established, we will apply the LCSM method to problems yet untreated by the LDA.

III. GaAs(001) SURFACE ENERGIES

A. The LCSM vs the LDA

The coefficients $\{\Delta\omega_M\}$ of the motif energies of Eq. (10) are listed in Table II for various octet bulk point defects and for (001) surface structures discussed in this paper. Results of *ab initio* LDA calculations[3–5] are given in the last column. Seven LDA energies are used to deduce the motif energies $\{\epsilon_M\}$ by equating the LCSM energy of Eq. (10) to the LDA energy. This is done in two steps: we first combine the four LDA-calculated GaAs bulk point defect energies (lines 1–4 in Table II) with Eq. (8). Using the bulk dielectric constant $\epsilon_b=13$, this gives the energies of five motifs: $\epsilon(Ga^{(4)})$, $\epsilon(As^{(4)})$, $\epsilon(Ga^{(3)})$, $\epsilon(As^{(3)})$, and ϵ(As-As), all expressed in terms of ϵ(Ga-Ga). Numerical values are given in Fig. 4. Second, we used three surface structures, $\beta 2(4\times2)$, $c(8\times2)$, and $c(2\times2)$ (see lines 11, 12, and 16 in Table II) to determine the remaining motif energy parameter $\epsilon(Ga^{(2)})$ and the effective *surface* dielectric constant ϵ_s. We need here three, instead of two, equations, because it appears that at the *surface* the As-As dimer bonds, and the As-As back bonds appearing in the $\gamma(2\times4)$ and $c(4\times4)$ structures in Figs. 1 and 2, have a different energy than bulk As-As bond. We obtain an energy difference of $\epsilon(\delta_{\text{As-As}})=-0.45$ eV, suggesting that the surface As-As bonds are strengthened with respect to bulk. No such effect is found for surface Ga-Ga bonds. The bottom halves of Figs. 1–3 show the point charges used in our Madelung sum. The fit to LDA yield a surface dielectric constant $\epsilon_s=8.1$. One may independently derive ϵ_s from classical electrodynamics,[11] using a GaAs bulk dielectric constant $\epsilon_b=13$. The result is $\epsilon_s=\epsilon_b+1/2=7$, in reasonable agreement with our fitted result of 8.1.

Having established the energies $\{\epsilon_M\}$ of the characteristic motifs and the effective surface dielectric constant ϵ_s, we can now use Eq. (10) to predict the energies of independent surface structures. Comparison of the LCSM results with the LDA results for structures *not used in the fit* (see entries in the next to the last column of Table II *not* marked "fitted") shows that the LCSM formation energies, with respect to the $\alpha(2\times4)$ surface, overestimate the LDA results (since all the errors are positive). The maximum error is 0.1 eV/(1×1) for the $\beta_{\rm rep}(4\times2)$ structure, while the minimum error is 0.0 eV/(1×1) for the $\alpha(4\times2)$ structure. Thus, the average LCSM error is ±0.05 eV/(1×1).

A graphic depiction of the $T=0$ GaAs(001) surface formation energies, with respect to the $\alpha(2\times4)$ surface is given in Fig. 5 as a function of the Ga chemical potential $\mu_{\rm Ga}$. It is essential for later calculations that the LCSM calculations

TABLE II. Coefficients that enter Eq. (10) are listed here for (i) point defects, (ii) (001) flat surfaces, and (iii) (001) surface steps of GaAs. The first eight columns give the frequency, $\omega_M(\boldsymbol{\sigma})-\omega_M(\boldsymbol{\sigma}_0)$ for the motifs indicated in the header [$\boldsymbol{\sigma}_0$=bulk GaAs for point defects, and $\boldsymbol{\sigma}_0=\alpha(2\times4)$ for flat surfaces. $\boldsymbol{\sigma}_0$ for steps is indicated after the name of each step structure]. ΔN_e is the coefficient of μ_e, while $\Delta N_{\mathrm{Ga}}-\Delta N_{\mathrm{As}}$ and $-\Delta N_{\mathrm{As}}$ are the coefficients for μ_{Ga} and ΔH, respectively. Columns 12–14 give, respectively, the Madelung energy ΔE_{Mad}, the LCSM formation energy $\Delta E^*=\Delta E-\Delta N_e\mu_e-(\Delta N_{\mathrm{Ga}}-\Delta N_{\mathrm{As}})\mu_{\mathrm{Ga}}$, and the corresponding LDA formation energy E^*_{LDA}. We use (—) to denote "not applicable" and NA to denote "not available." The seven entries denoted "fitted" were used to fit the LCSM results; all other ΔE values obtained by the LCSM are predicted, with no additional input.

		$\mathrm{Ga}^{(4)}$	$\mathrm{As}^{(4)}$	$\mathrm{Ga}^{(3)}$	$\mathrm{As}^{(3)}$	$\mathrm{Ga}^{(2)}$	Ga-Ga	As-As	$\delta_{\mathrm{As\text{-}As}}$	ΔN_e	$\Delta N_{\mathrm{Ga}}-\Delta N_{\mathrm{As}}$	$-\Delta N_{\mathrm{As}}$	$-\Delta E_{\mathrm{Mad}}$ (eV)	ΔE^* (eV)	$\Delta E^*_{\mathrm{LDA}}$ (eV)
							(i) Defects (per defect)								
1.	V_{Ga}^{3-}	−1	−4	0	4	0	0	0		−3	1	0	0.52	fitted	5.72
2.	V_{As}^{3+}	−4	−1	4	0	0	0	0		3	−1	−1	0.52	fitted	0.84
3.	$\mathrm{Ga}_{\mathrm{As}}^{2-}$	1	−1	0	0	0	4	0		−2	−2	−1	0	fitted	2.57
4.	$\mathrm{As}_{\mathrm{Ga}}^{2+}$	−1	1	0	0	0	0	4		2	2	1	0	fitted	1.85
							(ii) Surfaces (per 1×1)								
5.	$\alpha(2\times4)$	0	0	0	0	0	0	0	0	0	0	0	0	0	0
6.	$\alpha(4\times2)$	0	0	0	0	0	0	0	$-\frac{1}{4}$	0	0	0	0.00	0.12	0.12
7.	$\beta(2\times4)$	0	0	0	$\frac{1}{4}$	0	$-\frac{1}{4}$	$\frac{1}{8}$	$\frac{1}{8}$	0	$\frac{1}{4}$	$\frac{1}{4}$	−0.03	0.14	0.07
8.	$\beta2(2\times4)$	0	0	0	$\frac{1}{4}$	0	$-\frac{1}{4}$	$\frac{1}{8}$	$\frac{1}{8}$	0	$\frac{1}{4}$	$\frac{1}{4}$	−0.10	0.06	0.02
9.	$\beta(4\times2)$	0	0	$\frac{1}{4}$	0	0	$\frac{1}{8}$	$-\frac{1}{4}$	$-\frac{1}{4}$	0	$-\frac{1}{4}$	0	0.00	0.09	0.00
10.	$\beta_{\mathrm{rep}}(4\times2)$	0	0	$\frac{3}{8}$	$-\frac{1}{8}$	0	$\frac{1}{2}$	$-\frac{1}{4}$	$-\frac{1}{4}$	0	$-\frac{1}{2}$	$-\frac{1}{8}$	0.01	0.18	0.08
11.	$\beta2(4\times2)$	0	0	$\frac{1}{4}$	0	0	$\frac{1}{8}$	$-\frac{1}{4}$	$-\frac{1}{4}$	0	$-\frac{1}{4}$	0	−0.11	fitted	−0.03
12.	$c(8\times2)$	0	0	0	0	0	0	0	0	0	0	0	0.11	fitted	0.12
13.	$\gamma(2\times4)$	0	0	0	$\frac{1}{2}$	0	$-\frac{1}{4}$	$\frac{1}{2}$	$\frac{1}{2}$	0	$\frac{1}{2}$	$\frac{1}{2}$	−0.15	0.34	0.32
14.	$c(4\times4)$	0	0	$-\frac{1}{2}$	$\frac{3}{4}$	0	$-\frac{1}{4}$	$\frac{13}{8}$	$\frac{13}{8}$	0	$\frac{5}{4}$	$\frac{3}{4}$	−0.05	0.73	0.69
15.	2×1	$\frac{1}{2}$	0	$-\frac{1}{2}$	$\frac{1}{2}$	$\frac{1}{2}$	$-\frac{1}{4}$	$-\frac{1}{4}$	$-\frac{1}{4}$	0	0	$\frac{1}{2}$	−0.68	0.15	0.07
16.	$c(2\times2)$	$\frac{1}{2}$	0	$-\frac{1}{2}$	$\frac{1}{2}$	$\frac{1}{2}$	$-\frac{1}{4}$	$-\frac{1}{4}$	$-\frac{1}{4}$	0	0	$\frac{1}{2}$	−0.78	fitted	0.05
17.	$c(8\times6)$	0	0	$-\frac{1}{2}$	$\frac{7}{12}$	0	$-\frac{1}{4}$	$\frac{11}{8}$	$\frac{11}{8}$	0	$\frac{13}{12}$	$\frac{7}{12}$	0.05	0.62	NA
18.	2×6	$-\frac{1}{6}$	$-\frac{1}{6}$	$\frac{1}{6}$	$\frac{1}{6}$	0	$-\frac{1}{12}$	$-\frac{1}{12}$	$-\frac{1}{12}$	0	0	0	−0.14	0.03	NA
19.	8×7	0	0	$-\frac{3}{14}$	$\frac{13}{28}$	0	$-\frac{1}{4}$	$\frac{43}{56}$	$\frac{43}{56}$	0	$\frac{19}{28}$	$\frac{13}{28}$	−0.05	0.38	NA
20	8×3	0	0	$-\frac{1}{3}$	$\frac{7}{12}$	0	$-\frac{1}{4}$	$\frac{9}{8}$	$\frac{9}{8}$	0	$\frac{11}{12}$	$\frac{7}{12}$	−0.02	0.56	NA
							(iii) Surface steps (per 1×)								
21.	AI-1/$\beta2(2\times4)$	0	0	$\frac{1}{4}$	$-\frac{1}{8}$	0	$\frac{1}{4}$	$-\frac{5}{16}$	$-\frac{5}{16}$	0	$-\frac{3}{8}$	$-\frac{1}{8}$	−0.10	−0.08	NA
22.	BII-1/$\beta(2\times4)$	$-\frac{3}{8}$	$-\frac{3}{8}$	$\frac{1}{2}$	$\frac{3}{8}$	0	0	$-\frac{3}{16}$	$-\frac{3}{16}$	0	$-\frac{1}{8}$	0	−0.38	0.14	0.16
23	DBA ($S=0$)/$\beta2(2\times4)$	0	0	0	0	0	0	0	0	0	0	0	0.05	0.05	0.05

here reproduce well the sequence of stable surface energies over the entire physical range of μ_{Ga}. We see that they do: Going from As rich to Ga rich, the sequence $c(4\times4)\rightarrow\beta2(2\times4)\rightarrow\alpha(2\times4)\rightarrow\beta2(4\times2)$ is reproduced. We further see that the LCSM method also reproduces reasonably well the order of energies and the "crossing point" chemical potentials of the LDA calculation.

Experimentally, three distinct STM surface phases (i.e., α, β, and γ phases) have been observed[12–17] on GaAs(001)-(2×4) surfaces at different growth conditions. The β phase is the most stable.[13,17] Farrell and Palmstrom[12] suggested the following atomic structures in the topmost surface layer for these phases: (α) two As-As dimers; (β) three As-As dimers; and (γ) a single As-As dimer with a 90° rotation, with respect to the normal As-As dimer orientation in (α) and (β). Later experiments,[13] however, suggested that the β phase also has two As-As dimers *in the top-most surface layer*. Recent LDA total-energy calculations by Northrup and Froyen[3,4] revealed that the β phase, which is stable [see Fig. 5(a)] over a broad chemical-potential range -0.7 eV$>\mu_{\mathrm{Ga}}>-0.2$ eV, has a structure ($\beta2$) containing *two* As-As dimers at the top-most surface layer and a third dimer located two layers below (see Fig. 1). Recent STM and reflection high-energy electron-diffraction (RHEED) measurements by Hashizume *et al.*[17] have confirmed the calculation of Northrup and Froyen. Hashizume *et al.* further showed[17] that the γ phase is a mixed phase containing locally ordered $\beta2$ structures coexisting with disordered $c(4\times4)$ structures.

B. Interpretation of relative surface stabilities

Once the basic motif energies and point charges are determined, the LCSM method permits a simple *interpretation* of the stability of various surfaces in terms of point-ion electrostatics and motif frequencies. Figure 4 shows, however, that the fitted motif energies $\{\epsilon_M\}$ depend on an undetermined energy of one of the motifs [ϵ(Ga-Ga) in the case of Fig. 4]. Thus, the *individual* ϵ_M's are not known in absolute value, although the sum $\Sigma_M\omega_M\epsilon_M$ is well defined for any real physical process. To assist in the interpretation of surface stability, it then makes sense to transform the set $\{\epsilon_M\}$ into a set of renormalized, chemical-potential-dependent mo-

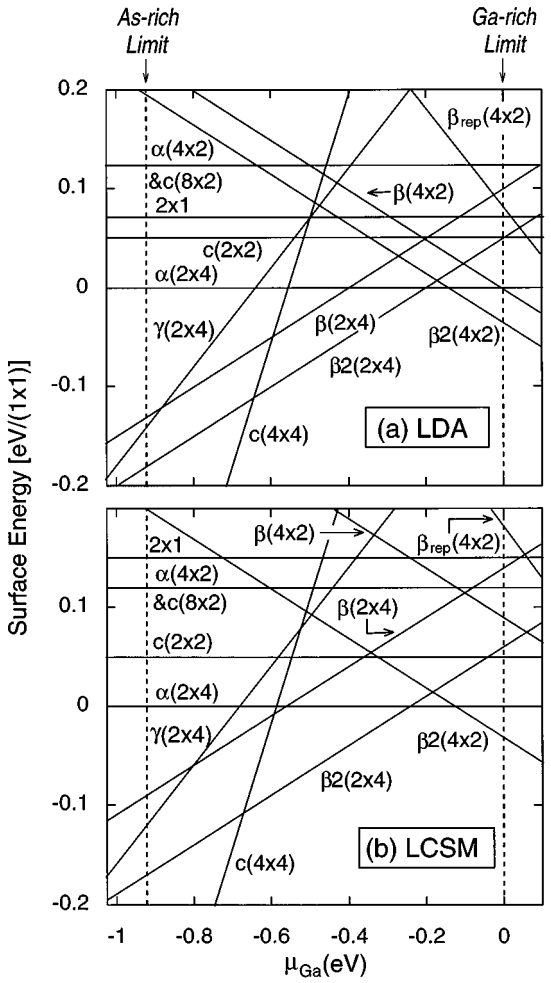

FIG. 5. GaAs(001) surface formation energies in units of (1×1) surface area are shown as a function of the Ga chemical potential: (a) LDA results from Refs. 3 and 4 and (b) present LCSM results. The energy of the $\alpha(2\times4)$ surface is used here as a reference. The range of the Ga chemical potential is indicated here by two vertical dashed lines at which either solid As or solid Ga will start to deposit on the surface, thus prohibiting any further change in μ_{Ga}.

tifs $\{\tilde{\epsilon}_M(\mu)\}$. The transformation is not unique; however, this does not matter since $\Sigma_M \omega_M \epsilon_M$ is invariant under the transformation. Table III gives our choice of the renormalized motifs labeled $M1$ to $M6$. Unlike the original motifs $\{\epsilon_M\}$ of Fig. 4, each of the renormalized motifs $\{\tilde{\epsilon}_M(\mu)\}$ corresponds to a formal reaction creating either an isolated bulk point defect or a defect pair: $M1$ is the motif for the creation of bulk GaAs from the Ga and As reservoirs, while $M2$, $M3$, $M4$, and $M5$ are, respectively, $\frac{1}{3}$ of the motif for creating a Ga-As vacancy pair, $\frac{1}{3}$ of the motif for creating a $\mathrm{Ga_{As}}$-$\mathrm{As_{Ga}}$ antisite pair, the motif for creating a $\mathrm{Ga_{As}^{(4)}}$ antisite, and the motif for creating a threefold-coordinated $\mathrm{Ga_{As}^{(3)}}$ antisite from bulk GaAs. $M6$ is not really a bulk motif, describing instead the creation of a twofold-coordinated $\mathrm{Ga^{(2)}}$ atom from a surface $\mathrm{Ga^{(3)}}$-$\mathrm{Ga^{(3)}}$ dimer. Unlike $\{\epsilon_M\}$, each of the *renormalized* motifs carries an absolute ''reaction energy.'' This is given in Table III.

Using the renormalized motifs $\{\tilde{\epsilon}_M\}$ for surfaces and surface defects, Eq. (10) simplifies to

$$\Delta E(\boldsymbol{\sigma},\mu_{\mathrm{Ga}}) = \sum_M \Delta\tilde{\omega}_M(\boldsymbol{\sigma})\tilde{\epsilon}_M(\mu_{\mathrm{Ga}}) + \Delta E_{\mathrm{Mad}}(\boldsymbol{\sigma}). \quad (11)$$

Considering the values of $\{\tilde{\epsilon}_M\}$ of Table III, we see that $M1$ is a ''neutral'' motif with $\tilde{\epsilon}_M=0$, while, with the exception of $\delta_{\mathrm{As\text{-}As}}$, the rest of the motifs have positive (i.e., destabilizing) energies. The motif energies, $\tilde{\epsilon}_M$, for $M6$, $M3$, and $M2$ in ascending order are 0.37, 1.10, and 1.37 eV, respectively. Recalling that $-0.92<\mu_{\mathrm{Ga}}<0$ eV in GaAs, we see that $\tilde{\epsilon}(M4)$ can be anywhere between $+2.57$ and $+4.59$ eV, while $\tilde{\epsilon}(M5)$ could be between $+0.71$ and $+2.55$ eV. In general, a given surface could be more stable than another if it has smaller $\Delta\tilde{\omega}_M$'s for the *high-energy* motifs, e.g., $M2$, and, for a large negative μ_{Ga}, $M4$, and $M5$. Using the LCSM language, we can now analyze some simple trends in previously calculated surface energies.

(i) Northrup and Froyen[4] and Garcia and Northrup[18] have recently discussed the relative stability of several surfaces in terms of the Madelung energy difference. Examples in Fig. 5 include the $\beta(2\times4)$ and $\beta2(2\times4)$, or the 2×1 and $c(2\times2)$ surfaces. Table III shows that these surface pairs have identical motifs (M) and identical motif frequencies ($\Delta\tilde{\omega}_M$) so, by Eq. (11), their energy difference is determined by the Madelung energy difference alone.

(ii) Figure 5 exhibits an apparent asymmetry between the As-terminated and the Ga-terminated surfaces: over a larger chemical potential range, the As-rich surfaces are more stable. Taking the transition between the As-terminated $\beta2(2\times4)$ to the Ga-terminated $\beta2(4\times2)$ surface as an example, we see that the transition occurs at $\mu_{\mathrm{Ga}}=-0.18$ eV, about 0.28 eV higher than the midpoint, $\mu_{\mathrm{Ga}}=-0.46$ eV, of the allowed Ga chemical potential window, $-0.92<\mu_{\mathrm{Ga}}<0$ eV. This asymmetry is caused by the strengthening of surface As-As bonds, $\epsilon(\delta_{\mathrm{As\text{-}As}})=-0.45$ eV: If we let $\epsilon(\delta_{\mathrm{As\text{-}As}})=0$, then the $\beta2(2\times4)$ to $\beta2(4\times2)$ transition would be at $\mu_{\mathrm{Ga}}=-0.52$ eV, much closer to the midpoint. One can see from Table II that all the Ga-rich surfaces [i.e., $\beta(4\times2)$, $\beta2(4\times2)$, $\beta_{\mathrm{rep}}(4\times2)$] and the surfaces with equal Ga and As coverages [i.e., $\alpha(4\times2)$, (2×1), $c(2\times2)$, and (2×6)] have *negative* $\Delta\omega_{\delta_{\mathrm{As\text{-}As}}}$ frequencies, while all the As-rich surfaces [i.e., $\beta(2\times4)$, $\beta2(2\times4)$, $\gamma(2\times4)$, $c(4\times4)$, $c(8\times6)$, 8×7, and 8×3] have *positive* $\Delta\omega_{\delta_{\mathrm{As\text{-}As}}}$.

(iii) Table III reveals remarkably simple regularities among the various flat GaAs(001) surface structures studied by LDA (Lines 1–12 in Table III): (a) With the exception of $\alpha(4\times2)$, the weights of the $M3$ and $\delta_{\mathrm{As\text{-}As}}$ motifs are equal. Hence, for most cases, we can group them into a single $(M3+\delta_{\mathrm{As\text{-}As}})$ motif with a motif energy $\tilde{\epsilon}(M3+\delta_{\mathrm{As\text{-}As}})=0.65$ eV. (b) With the exception of the 2×1 and $c(2\times2)$ surfaces, all other surfaces involve only three (out of six) renormalized motifs, i.e., $M2$, $(M3+\delta_{\mathrm{As\text{-}As}})$, and $M5$.

(iv) The energy difference between the stable As-terminated $\beta2(2\times4)$ and the Ga-terminated $\beta2(4\times2)$ surfaces can be written as

$$E[\beta2(2\times4)]-E[\beta2(4\times2)] = \tfrac{3}{8}\tilde{\epsilon}(M3+\delta_{\mathrm{As\text{-}As}}) - \tfrac{1}{4}\tilde{\epsilon}(M5) + \Delta E_{\mathrm{Mad}}, \quad (12)$$

or numerically,

TABLE III. Coefficients that enter Eq. (11) for (i) flat surfaces and (ii) surface steps of GaAs, using renormalized motifs ($M1$ to $M6$) and $\delta_{\text{As-As}}$. The relations between the renormalized motifs and those in Fig. 4 are given under the headers with the chemical potential dependence included.

Name:		$M1$ $Ga^{(4)}+As^{(4)}+\Delta H$	$M2$ $Ga^{(3)}+As^{(3)}+\Delta H$	$M3$ (Ga-Ga) +(As-As)	$M4$ $Ga^{(4)}-As^{(4)}+4$(Ga-Ga) $-2\mu_{Ga}-\Delta H$	$M5$ $Ga^{(3)}-As^{(3)}+3$(Ga-Ga) $-2\mu_{Ga}-\Delta H$	$M6$ $Ga^{(2)}-Ga^{(3)}$ $-$(Ga-Ga)/2	δ_{As-As}
Energy:		=0.0 (eV)	=1.37 (eV)	=1.10 (eV)	$=2.57-2\mu_{Ga}$ (eV)	$=0.71-2\mu_{Ga}$ (eV)	=0.37 (eV)	=−0.45 (eV)
				(i) Surfaces (per 1×1)				
1.	$\alpha(2\times4)$	0	0	0	0	0	0	0
2.	$\alpha(4\times2)$	0	0	0	0	0	0	$-\frac{1}{4}$
3.	$\beta(2\times4)$	0	$\frac{1}{8}$	$\frac{1}{8}$	0	$-\frac{1}{8}$	0	$\frac{1}{8}$
4	$\beta2(2\times4)$	0	$\frac{1}{8}$	$\frac{1}{8}$	0	$-\frac{1}{8}$	0	$\frac{1}{8}$
5.	$\beta(4\times2)$	0	$\frac{1}{8}$	$-\frac{1}{4}$	0	$\frac{1}{8}$	0	$-\frac{1}{4}$
6.	$\beta_{rep}(4\times2)$	0	$\frac{1}{8}$	$-\frac{1}{4}$	0	$\frac{1}{4}$	0	$-\frac{1}{4}$
7.	$\beta2(4\times2)$	0	$\frac{1}{8}$	$-\frac{1}{4}$	0	$\frac{1}{8}$	0	$-\frac{1}{4}$
8.	$c(8\times2)$	0	0	0	0	0	0	0
9.	$\gamma(2\times4)$	0	$\frac{1}{4}$	$\frac{1}{2}$	0	$-\frac{1}{4}$	0	$\frac{1}{2}$
10.	$c(4\times4)$	0	$\frac{1}{8}$	$\frac{13}{8}$	0	$-\frac{5}{8}$	0	$\frac{13}{8}$
11.	2×1	$\frac{1}{4}$	$\frac{1}{4}$	$-\frac{1}{4}$	$\frac{1}{4}$	$-\frac{1}{4}$	$\frac{1}{2}$	$-\frac{1}{4}$
12.	$c(2\times2)$	$\frac{1}{4}$	$\frac{1}{4}$	$-\frac{1}{4}$	$\frac{1}{4}$	$-\frac{1}{4}$	$\frac{1}{2}$	$-\frac{1}{4}$
13.	$c(8\times6)$	0	$\frac{1}{24}$	$\frac{11}{8}$	0	$-\frac{13}{24}$	0	$\frac{11}{8}$
14.	2×6	$-\frac{1}{6}$	$\frac{1}{6}$	$-\frac{1}{12}$	0	0	0	$-\frac{1}{12}$
15.	8×7	0	$\frac{1}{8}$	$\frac{43}{56}$	0	$-\frac{19}{56}$	0	$\frac{43}{56}$
16.	8×3	0	$\frac{1}{8}$	$\frac{9}{8}$	0	$-\frac{11}{24}$	0	$\frac{9}{8}$
				(ii) Surface steps (per 1×)				
17.	AI-1/$\beta2(2\times4)$	0	$\frac{1}{16}$	$-\frac{5}{16}$	0	$\frac{3}{16}$	0	$-\frac{5}{16}$
18.	BII-1/$\beta(2\times4)$	$-\frac{3}{8}$	$\frac{7}{16}$	$-\frac{3}{16}$	0	$\frac{1}{16}$	0	$-\frac{3}{16}$
19.	DBA ($S=0$)/$\beta2(2\times4)$	0	0	0	0	0	0	0

$$E[\beta2(2\times4)]-E[\beta2(4\times2)]=\tfrac{3}{8}\times0.65-\tfrac{1}{4}\,(0.71-2\mu_{\text{Ga}})+0.01(\text{eV}). \quad (13)$$

Since $\Delta E_{\text{Mad}}=0.01$ eV is negligible, the energy difference in Eq. (13) is determined by the energies of the $M3$ and $M5$ motifs: a positive $\tilde{\epsilon}(M3+\delta_{\text{As-As}})=0.65$ eV stabilizes the $\beta2(4\times2)$ surface, while a positive $\tilde{\epsilon}(M5)$ stabilizes, instead, the $\beta2(2\times4)$ surface. Recalling that μ_{Ga} is negative, the μ_{Ga} dependence of $\tilde{\epsilon}(M5)=0.71-2\mu_{\text{Ga}}$ (eV) increases the energy of $\beta2(4\times2)$, as one moves to Ga-poor (more negative μ_{Ga}) conditions, thus explaining the $\beta2(4\times2)$ to $\beta2(2\times4)$ transition.

Similarly, the energy difference between the $c(4\times4)$ and $\beta2(2\times4)$ surfaces can be written as

$$E[c(4\times4)]-E[\beta2(2\times4)]=\tfrac{3}{2}\tilde{\epsilon}(M3+\delta_{\text{As-As}})-\tfrac{1}{2}\tilde{\epsilon}(M5)+\Delta E_{\text{Mad}}. \quad (14)$$

With a ΔE_{Mad} of only 0.05 eV, again the interplay between $M3$ and $M5$ motif energies dominates the transition between the two structures.

(v) The (2×1) and $c(2\times2)$ structures have the most negative Madelung energies (see Table II), yet their formation energies are higher than that of the $\alpha(2\times4)$ surface. Table III provides the reason. It shows that among other things, the creation of the (2×1) and $c(2\times2)$ structures requires the conversion of $\frac{1}{4}$ of the relatively low-energy $M5$ motif into a relatively high-energy $M4$ motif, costing 0.47 eV. This offsets part of the ~0.7 eV more negative Madelung energies of the (2×1) and $c(2\times2)$ structures. It is interesting to note that the $M6$ motif (which is the only motif linked to surface $Ga^{(2)}$ atoms) does not greatly destabilize the (2×1) and $c(2\times2)$ surfaces per se.

IV. GaAs(001) SURFACE STRUCTURES UNEXPLORED BY THE LDA

Using the LCSM approach, we now explore surface structures for which the surface cell size can be too large to be handled efficiently with current LDA first-principles techniques. This includes (i) the disordered "2×3" surface,[19] (ii) the 2×6 surface,[20] and (iii) the mixed γ phase of the 2×4 surface.[17]

A. The "2×3" surface

Two 2×3 surface phases were observed[19] by RHEED during molecular-beam epitaxy growth, corresponding to approximate 0.9 (low) and 1.1 (high) ML As coverage. Gomyo *et al.*[21] recently observed that an (unspecified) 2×3 surface is responsible for a different type of *three* period ordering for $Al_{0.48}In_{0.52}As$ alloy on InP(001). They proposed a structural model for the 2×3 surface [Fig. 6(a)]. Since their reasoning for the ordering is rooted in the atomic-scale structure of the surface (in particular, the orientation and periodicity of the surface As-As dimers), one wonders whether the structural model proposed by Gomyo *et al.* represents a reasonably

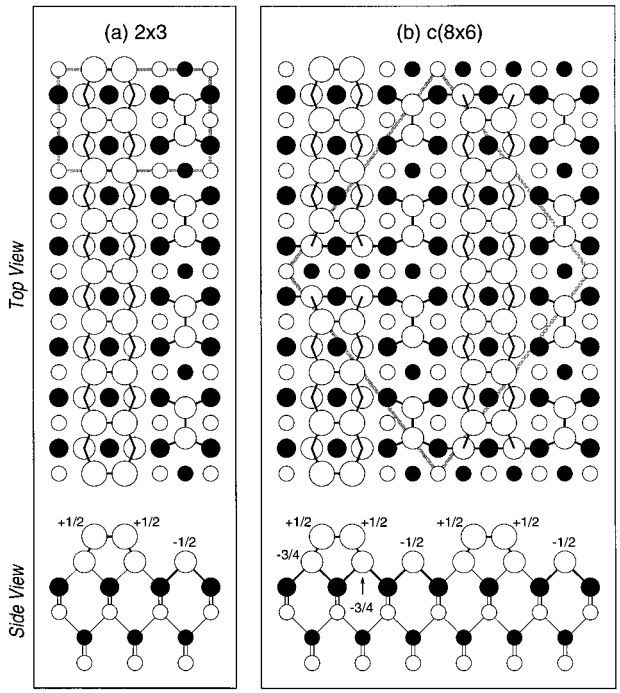

FIG. 6. Top and side views of the (2×3) surface structure, proposed by Gomyo *et al.* (Ref. 21), and the $c(8\times6)$ structure. The legends are the same as in Fig. 1.

stable surface. Unfortunately, following the octet rule, we see that this surface is not charge compensated (note the charge assignment at the bottom of Fig. 6), so this structure cannot be stable. Here, we modify the model of Gomyo *et al.* to achieve surface charge compensation. This is done by removing some of the surface As-As dimers. The resulting $c(8\times6)$ structure, containing 24 atoms per unit cell [see Fig. 6(b)], differs from the original model of Gomyo *et al.*, by having a missing As-As dimer for every eight dimers in a row. We suggest that the experimentally observed 2×3 surface could be a $c(8\times6)$ surface, which appears in the RHEED as 2×3, due to disorder of the missing dimers. The $c(8\times6)$ surface structure is stabilized (see Table III) by a high density of As-As adatom dimers on an As-terminated surface. Our LCSM calculation indicates that the ensuing $c(8\times6)$ structure has only slightly higher formation energies than the stable $c(4\times4)$ surface in the chemical-potential range surrounding the $c(4\times4)\rightarrow\beta2(2\times4)$ transition (see Fig. 7). Thus, a disordered $c(8\times6)$ (or 2×3) surface may exist at growth temperatures, due to entropy gain by surface disorder, but it could disappear as a stable surface structure *after* growth. The calculated surface As coverage for the $c(8\times6)$ surface is 1.0833 ML. This value is reasonably close to the observed[19] coverage for the high As coverage 2×3 surface, i.e., ~1.1 ML. In light of the similarity between the $c(8\times6)$ and the (2×3) surface models in Fig. 6 (in particular, the identical dimer orientation), we believe that the basic argument given by Gomyo *et al.* for the association of the three period ordering with such surface dimer orientation is still valid.

B. The 2×6 surface

Figure 8 shows the 2×6 surface structure proposed by Biegelsen *et al.*[20] based on their STM images. The 2×6 surface contains 12 atoms per unit cell. Similar to the $\alpha(2\times4)$ surface, the 2×6 surface has equal Ga and As coverage and its formation energy does not depend on the Ga chemical potential. The relative LCSM formation energy [per (1×1) surface] is

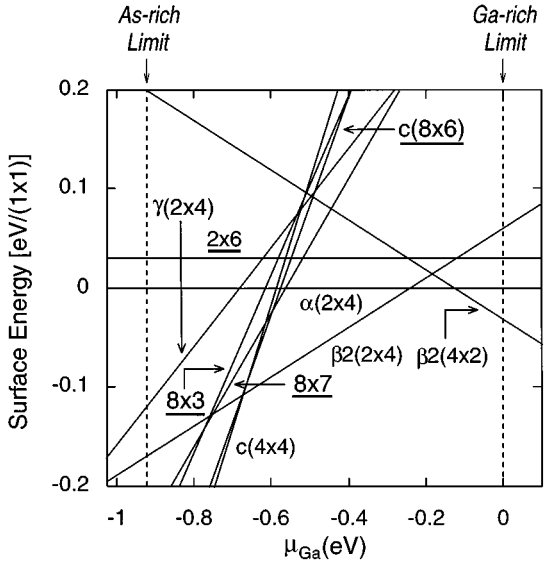

FIG. 7. Formation energy for GaAs(001)-$c(8\times6)$, -2×6, -8×7, and -8×3 surface structures (highlighted in the figure by underlines). The legends are the same as in Fig. 5.

$$E[(2\times6)]-E[\alpha(2\times4)]$$

$$=\tfrac{1}{6}\tilde{\epsilon}(M2)-\tfrac{1}{12}\tilde{\epsilon}(M3+\delta_{\text{As-As}})+\Delta E_{\text{Mad}}$$

$$=0.034\ \text{eV}. \tag{15}$$

We see that although the 2×6 surface has a $\frac{1}{12}$ lower density of the $(M3+\delta_{\text{As-As}})$ motif, the ensuing energy gain is not sufficient to offset the energy loss, due to $\frac{1}{6}$ higher density of the $M2$ motif. The net increase in the energy of motifs is, nevertheless, largely offset by the 0.14 eV decrease in the Madelung energy, due to a more even distribution of surface donor and acceptor charges. Thus, the 2×6 surface is only 0.03 eV higher in energy than the stable $\alpha(2\times4)$ surface. Experimentally, the 2×6 surface is obtained from the annealing of an As-rich $c(2\times8)$ surface [which is a variation of the $\beta2(2\times4)$ surface]. We, thus, expect that annealing drives off some of the surface As-As dimers. The observed 2×6 surface is also not completely ordered. This may be caused by the fact that the 2×6 surface is only metastable.

C. The $\gamma(2\times4)$ surface: The mixed phase of $\beta2(2\times4)$ and $c(4\times4)$ surfaces

Recently, Hashizume *et al.*[17] reexamined the $\gamma(2\times4)$ surface phase and concluded that it does not have the structure proposed earlier[12] (Fig. 1). Instead, Hashizume *et al.* proposed that the γ phase is a mixture of the two stable $\beta2(2\times4)$ and $c(4\times4)$ surfaces. Their STM images showed that the main feature of the mixed phase is the presence of open areas, whose widths are at least seven times that of a

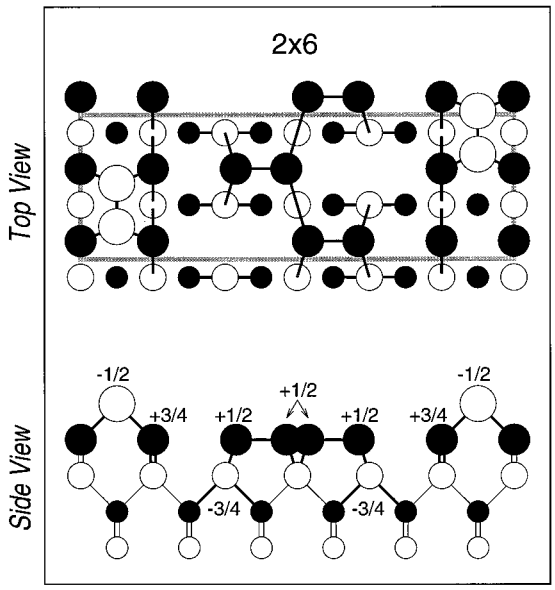

FIG. 8. Top and side views of the (2×6) surface structure proposed by Biegelsen *et al.* (Ref. 20). The legends are the same as in Fig. 1.

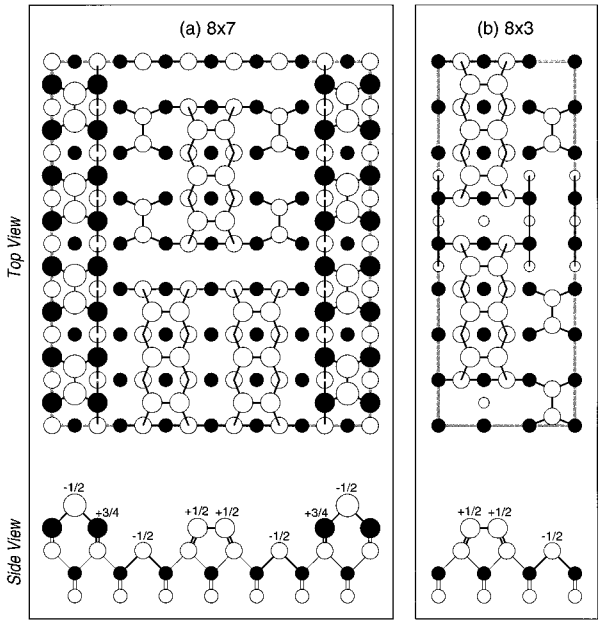

FIG. 9. Top and side views of the (8×7) and (8×3) surface structures. The legends are the same as in Fig. 1.

(1×1) cell (7×); only a small percentage of the surface has 5×, while smaller open areas are absent.

To see whether a structure resembling the mixed phase can have a lower energy than the $\gamma(2\times4)$ surface structure of Fig. 1, we constructed, starting from the two models suggested in Ref. 17, an 8×7 (=56 atoms per cell) surface structure with an open area of 7× [see Fig. 9(a)]. The 8×7 cell contains three $c(4\times4)$ surface cells and four $\beta2(2\times4)$ surface cells. While each $c(4\times4)$ cell has three As adatom dimers and one missing dimer as shown in Fig. 2, the $\beta2(2\times4)$ cells are deformed to fill the space left by the $c(4\times4)$ cells. This 8×7 structure is not the only structure that can be made from the $\beta2(2\times4)$ and $c(4\times4)$ surfaces. We can also make 8×9, 8×11, and similar structures. The smallest charge compensated supercell is the 8×5 cell, where the As-As dimers of the $\beta2(2\times4)$ cells in the open area in Fig. 9(a) become surface nearest neighbors. The 8×5 surface has a higher surface energy, due to Coulomb repulsion among these dimers. The motif frequencies for the 8×7 surface are shown in Table II, line 19 and in Table III, line 15. These motifs are, in fact, the average of the motif frequencies of three $c(4\times4)$ and four $\beta2(2\times4)$ surface cells. Thus, the energy difference between the 8×7 surface and the average of $c(4\times4)$ and $\beta2(2\times4)$ surfaces lies in the Madelung energy difference, which is higher for the 8×7 surface by about 0.026 eV/(1×1). This is expected, since we must sacrifice the Madelung energy in order for a complete space filling in the 8×7 surface. The energy of the 8×7 structure vs μ_{Ga} is shown in Fig. 7: It is *lower* than that of the $\gamma(2\times4)$ structure. In particular, at the chemical potential corresponding to the $c(4\times4)\rightarrow\beta2(2\times4)$ transition, the calculated energy of the 8×7 structure is about 0.06 eV/(1×1) lower. This confirms the work of Hashizume *et al.* Since the *real* 8×7 structure is disordered, its energy will be further lowered at finite temperatures, due to an entropy term. This may explain its apparent stability at growth temperatures.

The 8×7 surface has the As-As dimers on the top surface, while the As-As adatom dimers are all in the open area [see Fig. 9(a)]. An alternative of the mixed surface structure can have, instead, the As-As adatom dimers on the top surface, while the As-As dimers are in the open area. One such example is the 8×3 (=24 atoms per cell) surface shown in Fig. 9(b). This surface has a $c(4\times4)$ to $\beta2(2\times4)$ ratio of 2:1. Figure 7 shows that the energy of the 8×3 surface is also lower than that of the $\gamma(2\times4)$ structure in the As-rich regime. Hashizume *et al.* did not observe the 8×3 surface, so it is probably not a part of the $\gamma(2\times4)$ surface phase. However, the surface excess of As atoms for this surface is $\frac{11}{12}=0.917$ ML along with a 3× periodicity in the [110] direction, suggesting that its disordered version could be the $l(2\times3)$ surface observed by Norenberg and Koguchi[19] (see Sec. IV A).

Besides the above surface reconstructions, other GaAs(001) surface patterns were also observed by RHEED. These include,[22] going from As-rich to Ga-rich growth conditions, the As-rich ''disordered'' (4×4) [$d(4\times4)$] surface, the transitional 3×1 and 4×6 surfaces, and the Ga-rich 1×6 surface. It has been suggested[20,23] that the 2×6 model here would simulate the 1×6 and 4×6 surfaces rather well. The metastable character of the surface revealed by the present calculation also agrees with what is known about the 1×6 and 4×6 surfaces. On the other hand, the 3×1 surface may be the Ga-rich analog of the disordered As-rich 2×3 surface in Sec. IV A. At this stage, more structural information about the $d(4\times4)$ surface is required to determine the microscopic nature of this surface.

V. APPLICATION OF THE LCSM APPROACH TO STEPS ON THE GaAs(001) SURFACE

We next illustrate the application of the LCSM approach to GaAs(001)-2×4 *surface steps*. We will restrict ourselves to bilayer and double bilayer steps that can be made up out

of the structural motifs of Fig. 4 (extension to many more surface steps will be discussed elsewhere[24]). We further identify only those step structures that satisfy the charge-compensation octet rule. These are reasonable assumptions, since the nominally flat GaAs(001) surfaces that were used to extract the LCSM parameters involve local troughs, whose facets (see Figs. 1–3) are miniforms of the (001) surface monolayer steps and the bilayer steps discussed here.

The GaAs(001) surface is a polar surface with an atomic stacking sequence... Ga/As/Ga/As. The step height h in unit of monolayer spacing ($=a/4$, where a is the bulk lattice constant) can thus only be a multiple of 2, i.e., $h=2t$, where $t=1,2,...$. This ensures that the upper and lower terraces are identical, made, in this case, of the As-terminated 2×4 surfaces. Furthermore, the (001) surface has two orthogonal, inequivalent surface orientations ([110] and [1$\bar{1}$0]). This leads to two types of basic steps: the A step, with edges parallel to surface As-As dimers along the [110] direction, and the B step, with edges perpendicular to the dimers.

Steps created as a pure geometric construct, for example, the primitive AI, AII steps on a $\beta2(2\times4)$ surface and the BII step on a $\beta(2\times4)$ surface shown in Fig. 10, do not automatically satisfy the charge-compensation octet rule: the AI, AII, and BII steps have the charge $Q_{AI}=+0.25$, $Q_{AII}=-0.25$; and $Q_{BII}=-0.75$, respectively (in unit of absolute value of an electron charge). Charged steps are electrostatically unstable. Below, we will discuss charge-compensated (''derivative'') steps derived by modifying these ''primitive'' steps. Thus, the AI step will be altered to AI-1, the BII step will be altered to BII-1, etc. These changes, as will be seen below, will convert electrostatically unstable steps into stable steps.

We will compare LDA calculations with the predictions of the LCSM method. Due to computer limitation, however, we will study here via the LDA only two simple steps for which the supercell sizes are either comparable to, or only slightly larger than that of the 2×4 surface cell. A supercell scheme [see Appendix B (Refs. 25 and 26)] is used to calculate the reference LDA step energies.

A. The AI-1 step

The structure of the AI-1 step on a $\beta2(2\times4)$ surface is shown in Fig. 11(a). This step is stabilized relative to AI by adding one Ga atom to every four-step units in Fig. 10(a), forming a $Ga^{(3)}$ motif. As Appendix A shows, the charge of an atom depends on its nearest neighbors. In the case of the AI-1 step, the added $Ga^{(3)}$ atom not only brings to the step a charge of $Q=+\frac{1}{4}$ (Table I, line 7), but also alters the nearest-neighbor configurations of its two $As^{(3)}$ and one $Ga^{(4)}$ nearest-neighbor atoms, and thus their charge assignment. Using the rule of Table I, we find that the added $Ga^{(3)}$ atom *effectively* compensates four units of the AI step.

The predicted formation energy of the AI-1 step from the flat $\beta2(2\times4)$ surface (per unit step) is

$$E[AI-1]-E[\beta2(2\times4)]$$

$$=\tfrac{1}{16}\tilde{\epsilon}(M2)-\tfrac{5}{16}\tilde{\epsilon}(M3+\delta_{\text{As-As}})+\tfrac{3}{16}\tilde{\epsilon}(M5)+\Delta E_{\text{Mad}}$$

$$=-0.08-\tfrac{3}{8}\mu_{Ga}(\text{eV}). \quad (16)$$

We see that the formation of the AI-1 step results in a $\frac{1}{16}$ increase in the $M2$ motif and a $\frac{3}{16}$ increase in the $M5$ motif, and a larger, $\frac{5}{16}$ decrease in the $(M3+\delta_{\text{As-As}})$ motif. This is accompanied by a 0.10 eV decrease in the Madelung energy (see Table II, line 21). The relatively large $M5$ motif frequency ($\frac{3}{16}$) and motif energy (2.11–1.11 eV, for $-0.7\leqslant\mu_{\text{Ga}}\leqslant-0.2$ eV) is the main reason for the positive

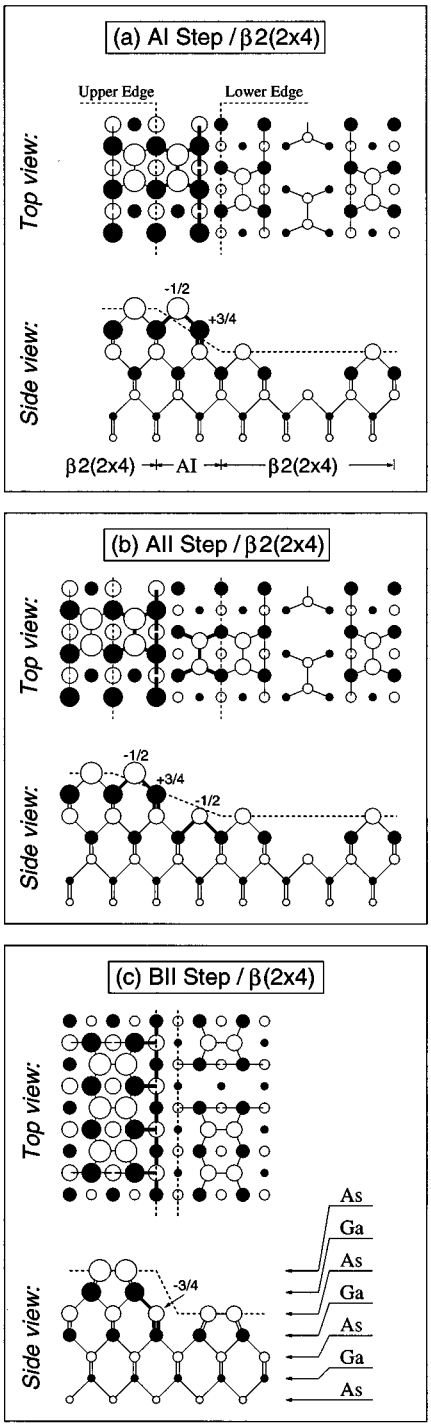

FIG. 10. Top and side views of the primitive GaAs(001) surface steps, depicted in a ball-stick model. The filled and open circles are Ga and As, respectively, with descending sizes from the top surface layer. Atomic bonds pertaining to steps are highlighted by thicker lines. In the side view, a dashed line is used to guide the eyes for viewing the step structure and the numbers by the atoms denote the charge assigned according to the octet rule (Table I).

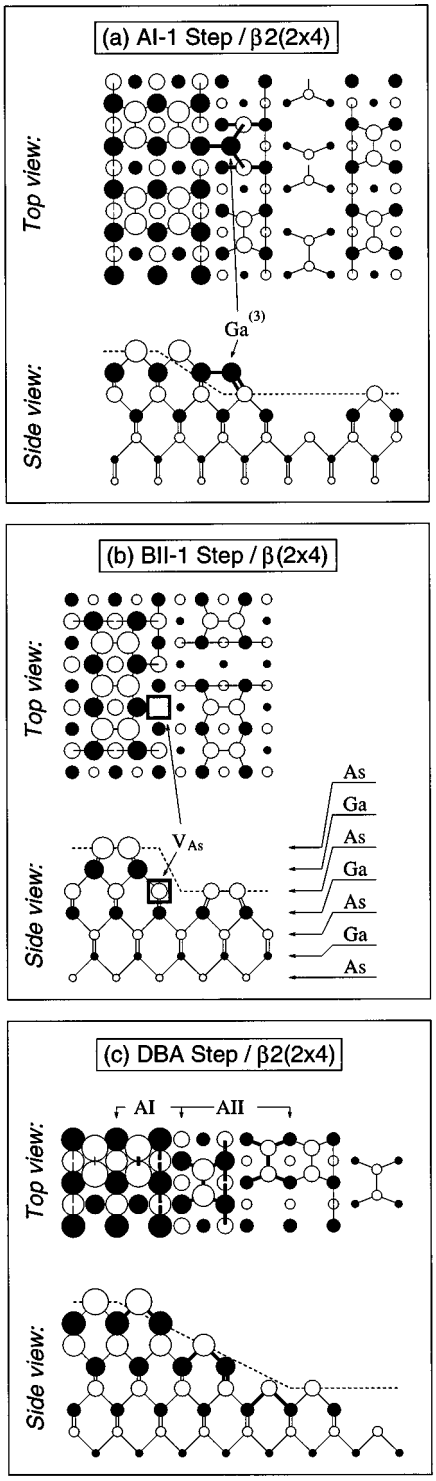

FIG. 11. Top and side views of charge compensated GaAs(001) steps. The square with a dark boundary indicates an As vacancy. The rest of the legends are the same as in Fig. 8.

formation energies of the AI-1 step for $\mu_{\mathrm{Ga}}<-0.21$ eV. No LDA calculation was performed here.

B. The BII-1 step

This is a B step on a $\beta(2\times4)$, not the $\beta2(2\times4)$, surface [Fig. 11(b)]. This step is stabilized with respect to BII by forming one $As^{(3)}$ vacancy for every four BII step units. The predicted LCSM formation energy of the BII-1 step from the $\beta(2\times4)$ surface (per unit step) is

$$E[BII-1]-E[\beta(2\times4)]=-\tfrac{3}{8}\tilde{\epsilon}(M1)+\tfrac{7}{16}\tilde{\epsilon}(M2)-\tfrac{3}{16}\tilde{\epsilon}(M3+\delta_{\text{As-As}})+\tfrac{1}{16}\tilde{\epsilon}(M5)+\Delta E_{\mathrm{Mad}}=0.14-\tfrac{1}{8}\mu_{\mathrm{Ga}}(\mathrm{eV}). \quad (17)$$

We see that the formation of the BII-1 step results in a $\frac{3}{8}$ decrease of the $M1$ motif [$\tilde{\epsilon}(M1)=0.0$ eV], but with a large, $\frac{7}{16}$ increase of the $M2$ motif [$\tilde{\epsilon}(M2)=1.37$ eV]. In comparison, the $-\frac{3}{16}$ change in the $(M3+\delta_{\text{As-As}})$ motif and the $\frac{1}{16}$ change in the $M5$ motif are relatively small. The high density of the $M2$ motif alone increases the formation energy by 0.6 eV, thus destabilizing the BII-1 step with respect to the $\beta(2\times4)$ surface. The large, positive energy of motifs of $0.52-\frac{1}{8}\mu_{\mathrm{Ga}}$ eV here is only partially offset by the decrease in the Madelung energy of 0.38 eV (see Table II, line 22).

Our LDA calculation showed that the BII-1 step is semiconducting with a band gap of $\sim$1 eV. The highest occupied states are the dangling-bond states of the step edge $As^{(3)}$ atoms and the lowest unoccupied states are the dangling-bond states of the $Ga^{(3)}$ atoms surrounding the $As^{(3)}$ vacancy. We obtain an LDA step formation energy (per unit step) of

$$E_{\mathrm{LDA}}[BII-1]-E_{\mathrm{LDA}}[\beta(2\times4)]=0.16-\tfrac{1}{8}\mu_{\mathrm{Ga}}(\mathrm{eV}), \quad (18)$$

close to the LCSM prediction [Eq. (17)].

C. The double $A(S=0)$ step on $\beta2(2\times4)$

The primitive AI step ($Q_{AI}=+0.25$) and AII step ($Q_{AII}=-0.25$) of Fig. 10 can be combined into charge-compensated surface structures, since $Q_{AI}+Q_{AII}\equiv0$. There are two ways to combine the two: (i) making a lower terrace from the AI step and a higher terrace from the AII step (or vise versa). This does not lead to a surface step per se, but rather to a surface groove. We denote by S [in unit of four surface atomic spacings $(4\times)$] the step separation. The $S=0$ case corresponds to the nominally flat $\beta2(2\times4)$ surface. (ii) Making both the AI and AII steps down steps (or up steps). This results in double bilayer height A (S) steps. Figure 11(c) shows the $S=0$ double A (DBA) step, which is the analog of the $S=0$ groove, i.e., the $\beta2(2\times4)$ surface. The LCSM formation energy for the DBA ($S=0$) step relative to the $\beta2(2\times4)$ surface (per unit step) is

$$E[\mathrm{DBA}(S=0)]-E[\beta2(2\times4)]=\Delta E_{\mathrm{Mad}}=0.05(\mathrm{eV}). \quad (19)$$

The $S=0$ double A step and a $\beta2(2\times4)$ surface unit cell have identical surface motifs and motif frequencies. Their energy difference is thus purely electrostatic. This energy is positive, due to a vertical separation between the AI and AII steps in the DBA ($S=0$) arrangement, which is zero in the $\beta2(2\times4)$ surface. Our LCSM calculations[24] reveal that while the formation energies of steps are positive, the DBA ($S=0$) and AI-1 steps are the two most stable surface A steps over the entire chemical-potential range of stable $\beta2(2\times4)$ surface ($-0.7<\mu_{\mathrm{Ga}}<-0.2$ eV). The DBA ($S=0$) step has the lowest step formation energy for $-0.7<\mu_{\mathrm{Ga}}<-0.29$ eV.

The LDA total-energy calculation showed that near the band gap, the electronic structure of the DBA ($S=0$) step is quite similar to that of the $\beta 2(2\times4)$ surface: both are semiconducting. The LDA step formation energy for the DBA ($S=0$) step (per unit step) is

$$E[\mathrm{DBA}(S=0)]_{\mathrm{LDA}}-E[\beta 2(2\times4)]_{\mathrm{LDA}}=0.05(\mathrm{eV}). \quad (20)$$

Comparison of the LCSM and LDA step formation energies [Eq. (17) vs Eq. (18) and Eq. (19) vs Eq. (20)] showed that the LCSM approach reproduces reasonably well the LDA-calculated step formation energies.

VI. SUMMARY

We have shown that an algebraic LCSM approach can be used for surface and surface step formation energies. The energy parameters in this approach are derived by fitting LCSM to a set of pseudopotential LDA total-energy calculations for a few *flat* GaAs(001) surfaces and for point defects in *bulk* GaAs. This set of parameters suffice to reproduce the energies of *other* (001) surfaces, calculated using the same LDA pseudopotential approach. Application of the LCSM method to the "2×3," 2×6 surfaces, and the γ phase of the (2×4) surface suggests that the As-rich $h(2\times3)$ surface may result from a disordered $c(8\times6)$ superstructure, while the 2×6 surface can be explained by the equal Ga and As coverage model proposed by Biegelsen *et al.* On the other hand, the γ phase is shown to be a mixture of the $\beta 2(2\times4)$ and $c(4\times4)$ surfaces. The potential for application of the LCSM method to predict formation energies of surface steps on the GaAs(001)-2×4 surfaces is also discussed. We find that at a tiny fraction of the computational cost, the LCSM approach can be applied to GaAs(001) surface steps, provided that these steps are made of the structural motifs of Fig. 4 (or Table III) and satisfy charge-compensation octet rule.

Like any other non-first-principles approach, one must decide from experience whether the LCSM approach with a given basis set of motifs can be applied to a particular surface problem. The leading approximation here is the truncation of the sum over motifs to a small number of terms (i.e., the first nearest neighbors), which also corresponds to the neglect of the interaction between motifs (an interaction that would have been represented by a larger-size motif in an untruncated expansion). The truncation implies also that the effects of strain are included via retentions of specifically strained motifs; we expect that a Keating-like valence force field approach can be implemented to account for different strain configurations without further expanding the basis of motifs.

ACKNOWLEDGMENTS

We thank S. Froyen and C. Wolverton for many helpful discussions on the subject, and D. E. Aspnes, T. Suzuki, J. E. Northrup, and D. J. Chadi for critical reading of the manuscript and useful comments. This work was supported by the Office of Energy Research (OER) [Division of Materials Science of the Office of Basic Science (BES)], U.S. Department of Energy, under Contract No. DE-AC36-83CH10093.

APPENDIX A: ASSIGNMENT OF POINT CHARGES TO GaAs SURFACES AND DEFECTS

The "electron counting" involved in establishing surface and defect charges given in Table I are illustrated here by examples. We consider first normal site atoms, i.e., Ga on a Ga site and As on an As site, as a continuation of the underneath bulk GaAs.

(i) *$Ga^{(4)}$ and $As^{(4)}$ atoms*. Ga has three valence electrons and a nuclear charge of +3. Fourfold-coordinated $Ga^{(4)}$ contributes, therefore, $\frac{3}{4}$ electron to each of its four bonds, thereby maintaining a *local* charge neutrality. Similarly, As has five valence electrons and a nuclear charge of +5; fourfold-coordinated $As^{(4)}$, thus, contributes $\frac{5}{4}$ electrons to its four bonds becoming also locally neutral. These can be written as lines 1 and 2 of Table I. In a bulk environment, each $Ga^{(4)}$ has four $As^{(4)}$ nearest neighbors and vice versa. Therefore, there are $\frac{3}{4}+\frac{5}{4}=2$ electrons per Ga-As bond, or eight electrons for the fourfold-coordinated GaAs. Thus, the octet rule is satisfied in the charge-neutral and semiconducting bulk GaAs.

It is a common practice of the electron counting model[8,7,4] to maintain the above bulk "partition rule" for both bulk and surface atoms: i.e., take Ga to contribute $\frac{3}{4}$ electron, and As to contribute $\frac{5}{4}$ electrons to each Ga-As bond. For bonds between like atoms (i.e., Ga-Ga and As-As bond), however, partition rules discussed below [(iv)–(vii)] become necessary.

(ii) *$Ga^{(3)}$ and $As^{(3)}$ atoms*. On the surface, one may have *threefold*-coordinated $Ga^{(3)}$. By the partition rule, the Ga contributes a total of $3\times\frac{3}{4}$ electrons to its three Ga-As bonds, leaving behind a $\frac{3}{4}$ electron in the fourth (dangling) bond. The previous calculation[7] showed that the dangling-bond orbital is located near the bulk CBM. The $Ga^{(3)}$ tends to empty this level, thus, becoming a $\frac{3}{4}$ electron donor with a net charge $Q=+\frac{3}{4}$ (in unit of e). Similarly, a threefold $As^{(3)}$ has $\frac{5}{4}$ electrons in its dangling-bond orbital near bulk VBM. By acquiring an additional $\frac{3}{4}$ electron, it will completely fill the dangling-bond level. Thus, $As^{(3)}$ is a $\frac{3}{4}$ electron acceptor, with a net charge $Q=-\frac{3}{4}$. Denoting in square brackets the nearest neighbors to an atom, this leads to lines 3 and 4 of Table I.

(iii) $Ga^{(2)}$ and $As^{(2)}$ atoms. The 2×1 and $c(2\times2)$ surfaces in Fig. 2 involve twofold-coordinated bridge site $Ga^{(2)}$. By the bulk partition rule, the $Ga^{(2)}$ contributes a $\frac{3}{4}$ electron to each of the two Ga-As bonds. So $Ga^{(2)}$ is a $3-2\times\frac{3}{4}=\frac{3}{2}$ electron donor ($Q=+\frac{3}{2}$). Similarly, twofold-coordinated $As^{(2)}$ is a $5-2\times\frac{3}{4}=\frac{5}{2}$ electron donor ($Q=+\frac{5}{2}$). (The latter charge assignment, however, has only nominal meaning as the $As^{(2)}$ motif is unstable; see Fig. 4.) This leads to lines 5 and 6 of Table I.

Often, two twofold-coordinated, second nearest-neighbor atoms of a GaAs(001) surface rebond to each other (or dimerize), thereby becoming threefold-coordinated, nearest neighbors (as evidenced in Figs. 1–3). In this case, the charge of the atom depends also on what the nearest neighbors are.

(iv) *Rebonded $Ga^{(3)}$ and $As^{(3)}$ atoms (Type I)*. Consider a surface $Ga^{(3)}$ atom bonded to two As and one $Ga^{(4)}$ [viz., the rebonded $Ga^{(3)}$ atoms in the $\alpha(2\times4)$ surface in Fig. 1]. Each of the two As atoms contributes $\frac{5}{4}$ electrons to its own Ga-As bond. The $Ga^{(3)}$ atom, thus, contributes $2\times\frac{3}{4}$ electrons to the

two Ga-As bonds. The bulk $Ga^{(4)}$ atom contributes, however, only $\frac{3}{4}$ electrons to the $Ga^{(3)}$-$Ga^{(4)}$ bond. The $Ga^{(3)}$ atom, thus, needs to contribute $\frac{5}{4}$ electrons to completely fill the $Ga^{(3)}$-$Ga^{(4)}$ bond. The dangling bond of the $Ga^{(3)}$ atom, thus, contains only $\frac{1}{4}$ electron. The $Ga^{(3)}$ atom is, therefore, a $\frac{1}{4}$, not a $\frac{3}{4}$, electron donor. Similarly, an $As^{(3)}$ atom with two Ga and one $As^{(4)}$ nearest neighbors [viz., the rebonded $As^{(3)}$ atoms in the $\alpha(4\times2)$ surface in Fig. 2] is a $\frac{1}{4}$, not a $\frac{3}{4}$, electron acceptor. This gives lines 7 and 8 of Table I.

(v) *Rebonded $Ga^{(3)}$ and $As^{(3)}$ atoms (Type II).* Another case involving rebonding is the surface $Ga^{(3)}$ atom in surface Ga-Ga dimers [viz., the Ga-Ga dimers in $\alpha(4\times2)$, $\beta(4\times2)$, $\beta_{\rm rep}(4\times2)$, $\beta2(4\times2)$, and $c(8\times2)$ surfaces in Figs. 2 and 3]. Here, a $Ga^{(3)}$ atom has two As and one $Ga^{(3)}$ nearest neighbors. By the bulk partition rule, this Ga atom contributes $2\times\frac{3}{4}=\frac{3}{2}$ electrons to the two Ga-As bonds. Each $Ga^{(3)}$ atom, on the other hand, must contribute one electron to the Ga-Ga bond, as the two $Ga^{(3)}$ atoms in a dimer are indistinguishable. This leaves behind $\frac{1}{2}$ electron in each of the $Ga^{(3)}$ gap states. Consequently, such a $Ga^{(3)}$ atom is not a $\frac{3}{4}$, but a $\frac{1}{2}$, electron donor. Similarly, an $As^{(3)}$ atom in an As-As dimer [viz., the As-As dimers in $\beta(2\times4)$, $\beta2(2\times4)$, $\gamma(2\times4)$, and $c(8\times2)$ surfaces in Figs. 1 and 3] is a $\frac{1}{2}$, not a $\frac{3}{4}$, electron acceptor. This gives lines 9 and 10 of Table I.

(vi) *Fourfold coordinated bulk antisites, $Ga_{As}^{(4)}$ and $As_{Ga}^{(4)}$ atoms.* When a Ga atom assumes the position of a bulk As atom, this Ga atom needs to contribute $\frac{5}{4}$ electrons to each of the four bonds. The $Ga_{As}^{(4)}$ atom has, however, only three valence electrons. To avoid electron deficiency in the bonds, the Ga antisite must accept two additional electrons ($Q=-2$). Conversely, an $As_{Ga}^{(4)}$ antisite is a two-electron donor ($Q=+2$). This leads to lines 11 and 12 of Table I.

(vii) *Threefold coordinated surface antisites, $Ga_{As}^{(3)}$ and $As_{Ga}^{(3)}$ atoms [viz., $\gamma(2\times4)$, $\beta_{rep}(4\times2)$, and $c(4\times4)$ surfaces in Figs. 1 and 2].* When a normal site $Ga^{(3)}$ atom ($Z=31$) is replaced by $As^{(3)}$ antisite ($Z=33$), an ionic charge $\Delta Q=33-31=+2$ will be added to the ion core. At the same time, two electrons ($\Delta Q=-2$) are also added to the empty dangling bond. This leads to $Q[{\rm As_{Ga}}]-Q[{\rm Ga_{Ga}}]=2-2=0$. The same is true for the $Ga^{(3)}$ antisites. These results can be written as lines 13 and 14 of Table I.

APPENDIX B: DETAILS OF THE LDA SUPERCELL APPROACH FOR CALCULATING STEP ENERGIES

The LDA formation energy of a step $\boldsymbol{\sigma}$ with respect to the flat surface ($\boldsymbol{\sigma}_0$) is defined as

$$\Delta E_{\rm LDA}(\boldsymbol{\sigma};\mu_{\mathscr{R}})=\Delta E^{*}_{\rm LDA}(\boldsymbol{\sigma})+\Delta E_{\mathscr{R}}(\boldsymbol{\sigma},\mu_{\mathscr{R}}), \quad \text{(B1)}$$

where the first term is the LDA energy difference between $\boldsymbol{\sigma}$ and $\boldsymbol{\sigma}_0$, *without* particle conservation, i.e.,

$$\begin{aligned}\Delta E^{*}_{\rm LDA}(\boldsymbol{\sigma})&=\Delta E_{\rm LDA}(\boldsymbol{\sigma};\mu_{\mathscr{R}})-\Delta E_{\mathscr{R}}(\boldsymbol{\sigma},\mu_{\mathscr{R}})\\&=\mathscr{E}(\boldsymbol{\sigma})-\mathscr{E}(\boldsymbol{\sigma}_0).\end{aligned} \quad \text{(B2)}$$

The second term is the reservoir energy,

$$\begin{aligned}\Delta E_{\mathscr{R}}(\boldsymbol{\sigma},\mu_{\mathscr{R}})&=\Delta N_{\rm Ga}\mu_{\rm Ga}+\Delta N_{\rm As}\mu_{\rm As}\\&=(\Delta N_{\rm Ga}-\Delta N_{\rm As})\mu_{\rm Ga}-\Delta N_{\rm As}\Delta H,\end{aligned} \quad \text{(B3)}$$

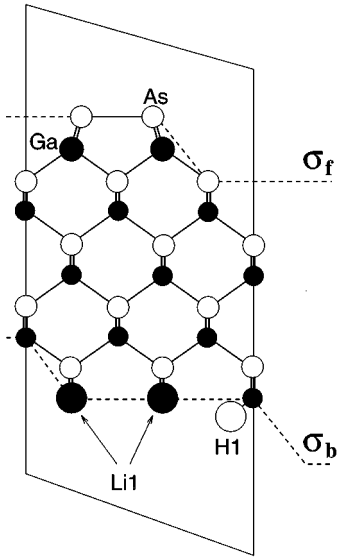

FIG. 12. A schematical drawing of the supercell used in the LDA calculation. The dashed lines in the figure indicate the locations of the front ($\boldsymbol{\sigma}_f$) and back ($\boldsymbol{\sigma}_b$) stepped surfaces.

of Eq. (9) at $\Delta N_e\mu_e=0$. We used in our calculation a *tilted* supercell (see Fig. 12), rather than the rectangular-shaped cells. The tilted cell contains one step on each side of the slab, whereas the rectangular cell contains two steps on one side of the slab with a *flat* back surface. For a fixed step separation on the surface, the volume of the tilted cell is about half of the rectangular cell. However, due to the polar nature of GaAs (001) surface, it is not possible to make the two steps in the tilted cell equivalent, i.e., $\boldsymbol{\sigma}_f\neq\boldsymbol{\sigma}_b$. In our calculation, we study the front surface, while the back surface is passivated by fictitious atoms. This involves an H1 ''atom,'' with no atomic core and a Li1 ''atom'' with a He core, carrying $+1.25$ and $+1.5$ ionic charges, respectively. Their potentials are generated in the same way as that for actual ions. The use of the fictitious atoms has negligible effects on step energies. The largest supercell used in the calculation has about 100 atoms and has a volume (including the vacuum region) equal to the volume of about 70 bulk GaAs unit cells. All atoms are fully relaxed according to their forces, except for the two outermost back surface layers, which are kept fixed. A valence force field approach[25] was used to check that the residual forces on the back surface atoms are negligible. Our calculation employs the Troullier-Martins soft-core pseudopotential,[26] with a plane-wave basis. Kinetic energy cutoffs ($E_{\rm cut}$) up to 10 Ry were used. We estimated that the errors will not exceed ±0.05 eV/(1×).

To extract $\mathscr{E}(\boldsymbol{\sigma})$ in Eq. (B2) from the above supercell approach, we assume that the front surface $\boldsymbol{\sigma}_f$ ($=\boldsymbol{\sigma}$ and $\boldsymbol{\sigma}_0$, respectively) and the back surface $\boldsymbol{\sigma}_b$ do not interact with each other, so that

$$\mathscr{E}(\boldsymbol{\sigma}_f+\boldsymbol{\sigma}_b)=\mathscr{E}(\boldsymbol{\sigma}_f)+\mathscr{E}(\boldsymbol{\sigma}_b). \quad \text{(B4)}$$

This allows us to write Eq. (B2) as

$$\mathscr{E}(\boldsymbol{\sigma})-\mathscr{E}(\boldsymbol{\sigma}_0)=[\mathscr{E}(\boldsymbol{\sigma}+\boldsymbol{\sigma}_{b1})-\mathscr{E}(\boldsymbol{\sigma}_0+\boldsymbol{\sigma}_{b2})] -[\mathscr{E}(\boldsymbol{\sigma}_{b1})-\mathscr{E}(\boldsymbol{\sigma}_{b2})], \quad \text{(B5)}$$

where $\boldsymbol{\sigma}_{b1}$ and $\boldsymbol{\sigma}_{b2}$ are two different back surface configurations. Different from the front surfaces, the back surfaces are only intermediate steps towards the final results. They can, thus, be made as simple as possible, i.e., the $(1\times)$ step and 1×1 surface. These allow us to use standard rectangular-shaped cells, with much larger step separations to evaluate accurately the second term in Eq. (B5).

[1] P. Boguslawski, Q. M. Zhang, Z. Zhang, and J. Bernholc, Phys. Rev. Lett. **72**, 3694 (1994).
[2] T. Ohno, Phys. Rev. Lett. **70**, 631 (1993).
[3] J. E. Northrup and S. Froyen, Phys. Rev. Lett. **71**, 2276 (1993).
[4] J. E. Northrup and S. Froyen, Phys. Rev. B **50**, 2015 (1994).
[5] S. B. Zhang and J. E. Northrup, Phys. Rev. Lett. **67**, 2339 (1991); J. E. Northrup and S. B. Zhang, Phys. Rev. B **47**, 6791 (1993); **50**, 4962 (1994).
[6] M. D. Pashley, Phys. Rev. B **40**, 10 481 (1989).
[7] D. J. Chadi, J. Vac. Sci. Technol. A **5**, 834 (1987).
[8] M. D. Pashley, K. W. Haberen, W. Friday, J. M. Woodall, and P. D. Kirchner, Phys. Rev. Lett. **60**, 2176 (1988).
[9] We use as reference for Eq. (5) bulk GaAs for point defects, the $\alpha(2\times4)$ surface for flat surfaces.
[10] We, thus, envision the case where a GaAs surface or bulk point defect exists in equilibrium with bulk GaAs and a (abstract) reservoir $\mathscr{R}$ serving as a source or drain for Ga, As atoms and electrons.
[11] J. D. Jackson, *Classical Electrodynamics*, 2nd ed. (Wiley, New York, 1975).
[12] H. H. Farrell and C. J. Palmstrom, J. Vac. Sci. Technol. B **8**, 903 (1990).
[13] E. J. Heller and M. G. Lagally, Appl. Phys. Lett. **60**, 2675 (1992).
[14] H. Xu, T. Hashizume, and T. Sakurai, Jpn. J. Appl. Phys. **32**, 1511 (1993).
[15] V. Bressler-Hill, M. Wassermeier, K. Pond, R. Maboudian, G. A. D. Briggs, P. M. Petroff, and W. H. Weinberg, J. Vac. Sci. Technol. B **10**, 1881 (1992).
[16] Y. Haga, S. Miwa, and E. Morita, J. Vac. Sci. Technol. B **12**, 2107 (1994).
[17] T. Hashizume, Q. K. Xue, J. Zhou, A. Ichimiya, and T. Sakurai, Phys. Rev. Lett. **73**, 2208 (1994).
[18] A. Garcia and J. E. Northrup, J. Vac. Sci. Technol. **12**, 2678 (1994).
[19] H. Norenberg and N. Koguchi, Surf. Sci. **296**, 199 (1993).
[20] D. K. Biegelsen, R. D. Bringans, J. E. Northrup, and L.-E. Swartz, Phys. Rev. B **41**, 5701 (1990).
[21] A. Gomyo, K. Makita, I. Hino, and T. Suzuki, Phys. Rev. Lett. **72**, 673 (1994).
[22] I. Kamiya, D. E. Aspnes, H. Tanaka, L. T. Florez, M. A. Koza, R. Bhat, and J. P. Harbison, Philos. Trans. R. Soc. London Ser. A **344**, 443 (1993).
[23] D. E. Aspnes (private communication).
[24] S. B. Zhang and A. Zunger (unpublished)
[25] J. E. Bernard, S. Froyen, and A. Zunger, Phys. Rev. B **44**, 11 178 (1991).
[26] N. Troullier and J. L. Martins, Phys. Rev. B **43**, 1993 (1991).